



Cite this: *Phys. Chem. Chem. Phys.*,  
2017, **19**, 29963

## Theoretical study on the gas adsorption capacity and selectivity of CPM-200-In/Mg and CPM-200-In/Mg-X ( $-X = -\text{NH}_2, -\text{OH}, -\text{N}, -\text{F}$ )<sup>†</sup>

Xiao-le Liu,<sup>a</sup> Guang-hui Chen, \*<sup>a</sup> Xiu-Jun Wang,<sup>\*b</sup> Peng Li,<sup>a</sup> Yi-bing Song<sup>a</sup> and Rui-yan Li<sup>c</sup>

The adsorption capacities of a heterometallic metal–organic framework (CPM-200-In/Mg) to VOCs (HCHO, C<sub>2</sub>H<sub>4</sub>, CH<sub>4</sub>, C<sub>2</sub>H<sub>2</sub>, C<sub>3</sub>H<sub>8</sub>, C<sub>2</sub>H<sub>6</sub>, C<sub>2</sub>H<sub>3</sub>Cl, C<sub>2</sub>H<sub>2</sub>Cl<sub>2</sub>, CH<sub>2</sub>Cl<sub>2</sub> and CHCl<sub>3</sub>) and some inorganic gas molecules (HCN, SO<sub>2</sub>, NO, CO<sub>2</sub>, CO, H<sub>2</sub>S and NH<sub>3</sub>), as well as its selectivity in ternary mixture systems of natural gas and post-combustion flue gas are theoretically explored at the grand canonical Monte Carlo (GCMC) and density functional theory (DFT) levels. It is shown that CPM-200-In/Mg is suitable for the adsorption of VOCs, particularly for HCHO (up to 0.39 g g<sup>-1</sup> at 298 K and 1 bar), and the adsorption capacities of some inorganic gas molecules such as SO<sub>2</sub>, H<sub>2</sub>S and CO<sub>2</sub> match well with the sequence of their polarizability (SO<sub>2</sub> > H<sub>2</sub>S > CO<sub>2</sub>). The large adsorption capacities of HCN and HCHO in the framework result from the strong interaction between adsorbates and metal centers, based on analyzing the radial distribution functions (RDF). Comparing C<sub>2</sub>H<sub>4</sub> and CH<sub>4</sub> molecules interacting with CPM-200-In/Mg by VDW interaction, we speculate that the high adsorption capacities of their chlorine derivatives in the framework could be due to the existence of halogen bonding or strong electrostatic and VDW interactions. It is found that the basic groups, including  $-\text{NH}_2$ ,  $-\text{N}$  and  $-\text{OH}$ , can effectively improve both the adsorption capacities and selectivity of CPM-200-In/Mg for harmful gases. Note that the adsorption capacity of CPM-200-In/Mg-NH<sub>2</sub> (site 2) (245 cm<sup>3</sup> g<sup>-1</sup>) for CO<sub>2</sub> exceeded that of MOF-74-Mg (228 cm<sup>3</sup> g<sup>-1</sup>) at 273 K and 1 bar and that for HCHO can reach 0.41 g g<sup>-1</sup>, which is almost twice that of 438-MOF and nearly 45 times of that in active carbon. Moreover, for natural gas mixtures, the decarburezation and desulfurization abilities of CPM-200-In/Mg-NH<sub>2</sub> (site 2) have exceeded those of the MOF-74 series, while for post-combustion flue gas mixtures, the desulfurization ability of CPM-200-In/Mg-NH<sub>2</sub> (site 2) is still comparable to those of the MOF-74 series at 303 K and 4 MPa. We hope that the current theoretical study could guide experimental research in the future.

Received 8th September 2017,  
Accepted 18th October 2017

DOI: 10.1039/c7cp06141b

rsc.li/pccp

<sup>a</sup> Department of Chemistry, Shantou University, Guangdong 515063, China.  
E-mail: ghchen@stu.edu.cn

<sup>b</sup> Key Laboratory of Functional Molecular Engineering of Guangdong Province, School of Chemistry and Chemical Engineering, South China University of Technology, Guangzhou 510640, China. E-mail: xjwangcn@scut.edu.cn

<sup>c</sup> College of Chemistry and chemical engineering of Inner Mongolia University for Nationalities, Tongliao 028043, China

<sup>†</sup> Electronic supplementary information (ESI) available: Table S1 contains XYZ coordinate of the CPM-200-In/Mg-NH<sub>2</sub>(site2). Table S2, S3 contains LJ potential parameters. Fig. S1 shows the snapshots of VOCs adsorbed in framework. Fig. S2 displays the Radial distribution functions  $g(r)$ . Fig. S3 shows Isosteric heats of VOCs adsorbed in CPM-200-In/Mg at 298 K. Fig. S4 displays the VDW (a, b) and Coulomb (c) interactions between the host and adsorbate. Fig. S5 shows adsorption selectivities of MOFs in CO<sub>2</sub>-H<sub>2</sub>S-CH<sub>4</sub> (a, b) and CO<sub>2</sub>-SO<sub>2</sub>-N<sub>2</sub> (c, d). Fig. S6 contains the CO<sub>2</sub> absorption capacity of MOFs. Fig. S7 displays the effect of temperature on gas selectivity of materials in CO<sub>2</sub>-H<sub>2</sub>S-CH<sub>4</sub> (a, b) and SO<sub>2</sub>-CO<sub>2</sub>-N<sub>2</sub> (c, d). See DOI: 10.1039/c7cp06141b

## 1. Introduction

Concerning the energy crisis and the aggravation of environmental pollution, effective control of air pollutants emission has become particularly critical and urgent. VOCs (volatile organic compounds *e.g.* HCHO, CHCl<sub>3</sub>, CH<sub>2</sub>Cl<sub>2</sub>, C<sub>2</sub>H<sub>2</sub>, C<sub>2</sub>H<sub>4</sub>, C<sub>2</sub>H<sub>6</sub>, C<sub>3</sub>H<sub>8</sub>, C<sub>2</sub>H<sub>2</sub>Cl<sub>2</sub> and C<sub>2</sub>H<sub>3</sub>Cl), components of acid rain (*i.e.* CO<sub>2</sub>, SO<sub>2</sub>, HCN and H<sub>2</sub>S) and automotive exhaust gases like NO and CO are major air pollutants that not only have serious impact on the environment but also pose great threats to human health. Therefore, the removal of these harmful gases from the atmosphere is a key issue. It is worth noting that increasing the desulfurization and decarbonization of mixture gases is also an important issue for protecting our environment. It is well known that both natural gas and biogas have methane (CH<sub>4</sub>) as their major component; however, it is often mixed with harmful gases like hydrogen sulfide (H<sub>2</sub>S) and carbon dioxide (CO<sub>2</sub>). It is alarming

that even a small amount of H<sub>2</sub>S in biogas has a harmful impact on the utilization of biogas.<sup>1</sup> Therefore, concerning the purity, harmful combustion products and the serious corrosion of equipment, H<sub>2</sub>S and CO<sub>2</sub> need to be removed before the gas is used. Apart from N<sub>2</sub>, the post-combustion flue gas also mainly contains SO<sub>2</sub> and CO<sub>2</sub>, which can cause acid rain; therefore, the exploration of materials for desulfurization and decarbonization is necessary.

Porous materials are thought to be promising adsorbents due to their high absorption capacity and selectivity for harmful gases. Among them, metal–organic frameworks (MOFs) are a new family of nanoporous materials that have received tremendous interest in the past few decades, owing to their great potential for H<sub>2</sub> storage,<sup>2</sup> CO<sub>2</sub> capture,<sup>3</sup> catalysis,<sup>4</sup> gas separation and purification<sup>5</sup> and so on; most of them have great chemical, thermal and mechanical stability. In addition, their functionalized counterparts have attracted considerable attention because they are more effective at gas separation<sup>6</sup> and adsorption.<sup>7</sup> More recently, the practical applications of MOF or porous coordination polymers (PCPs) have been recognized for air quality management (AQM)<sup>8</sup> due to their outstanding properties in gas capture and separation,<sup>8,9</sup> and the influencing factors of gas adsorption such as pore volume<sup>10</sup> and interaction mechanism<sup>9,11</sup> have been broadly investigated. MOFs have also been used in our daily life; for example, BASF has realized the commercial utilization of MOFs such as Cu-BTC, Fe-BTC, ZIF-8, MOF-177, IRMOF-8, etc., and some of them can effectively remove harmful and toxic chemicals.<sup>12</sup>

Recently, a new type of heterometallic MOF with excellent performance for CO<sub>2</sub> capture (CPM-200s) was synthesized by Zhai *et al.*,<sup>13</sup> the capacity of which was close to the all-time record set by MOF-74-Mg (228 cm<sup>3</sup> g<sup>-1</sup>, 273 K, 1 bar). The concept of heterometallic MOFs is by no means new, and the challenge is how to deal with the perceived impossibilities of combining metals to create high performance materials.<sup>13</sup> Synergy between heterometals would most likely occur through the most intimate form of integration.<sup>13</sup> Such an intimate form of integration between dissimilar metals allows both fine and dramatic tuning of their properties across a large range and all within the same framework type. For example, compared with homometallic CPM-200-In (109.6 cm<sup>3</sup> g<sup>-1</sup>, 273 K, 1 bar), the CO<sub>2</sub> adsorption capacity of heterometallic CPM-200-In/Mg (190.8 cm<sup>3</sup> g<sup>-1</sup>, 273 K, 1 bar) is dramatically promoted.<sup>13</sup> In this work, to highlight the unique significance of main-group metals in the design of high-performance materials for gas adsorption and separation, we will use CPM-200-In/Mg as an example to investigate its adsorption capacity for VOCs (HCHO, C<sub>2</sub>H<sub>4</sub>, CH<sub>4</sub>, C<sub>2</sub>H<sub>2</sub>, C<sub>3</sub>H<sub>8</sub>, C<sub>2</sub>H<sub>6</sub>, C<sub>2</sub>H<sub>3</sub>Cl, C<sub>2</sub>H<sub>2</sub>Cl<sub>2</sub>, CH<sub>2</sub>Cl<sub>2</sub> and CHCl<sub>3</sub>) and some harmful inorganic gases (HCN, SO<sub>2</sub>, NO, CO<sub>2</sub>, CO, H<sub>2</sub>S and NH<sub>3</sub>) as well as their desulfurization and decarbonization abilities in post-combustion flue gas and natural gas.

## 2. Computational methods

### 2.1 Structure

From the previous work of Zhai *et al.*,<sup>13</sup> we know that CPM-200s have superior CO<sub>2</sub> uptake capacity, particularly for CPM-200-In/Mg

and CPM-200-Fe/Mg. Considering that heterometallic CPM-200-In/Mg has high adsorption capacity for gas molecules with large polarizability and most of the absorbed molecules we investigated are acidic, we introduced the –F atom and some basic groups (–OH and –NH<sub>2</sub>) to the MOF, which have proved to be effective in enhancing the gas absorption and (or) selectivity of the materials,<sup>14,15</sup> and we denoted the functionalized MOFs as CPM-200-In/Mg–X. As the pyridine ring is of greater polarity and alkalinity than the benzene ring, we introduced the pyridine ring for functionalization instead of the benzene ring and also denoted this new material as CPM-200-In/Mg–N for convenience.

Furthermore, from Qiao's work<sup>16</sup> we know that the increase in the amine number can enhance the selectivity of materials, but it always reduces the adsorption capacity of MOFs as the amine functional groups grafted into MOFs reduces their free volume. Moreover, Qiao<sup>16</sup> also proved that UIO-67, whose lattice parameters and organic ligands are similar to those of CPM-200-In/Mg, has the largest adsorption ability when grafted with one amine group (–NH<sub>2</sub> or –NHCOH) rather than having one more amine group, compared to the original; at the same time it also has larger selectivity than the original. Similarly, we introduced different functional groups to CPM-200-In/Mg, such as –N, –OH, –NH<sub>2</sub> and –F, independently to test their effects on the adsorption capacity and separation behavior of the materials. The relation between adsorption and separation abilities and different substitution sites of –NH<sub>2</sub> were also tested, which was not studied before. All the structure models are shown in Fig. 1.

The structure of CPM-200-In/Mg was theoretically constructed according to the experimental data, which was gathered from single-crystal X-ray diffraction.<sup>13</sup> The functionalized structures of CPM-200-In/Mg–X (X = –F, –NH<sub>2</sub> (site 1, site 2), –OH) were constructed by replacing the H atoms of benzene rings with corresponding functional groups, while the CPM-200-In/Mg–N was obtained by replacing the benzene rings with pyridine rings. The periodic density functional theory (DFT) for MOF geometrical optimization was then carried out to further relax the functionalized structures by using DMol<sup>3</sup> incorporated in the Material Studio program package.<sup>17,18</sup> The GGA/PBE functional combined with the double numerical basis set containing the polarization function (DNP) were employed. The structural features of the CPM-200-In/Mg series are listed in Table 1, and the XYZ coordinates of CPM-200-In/Mg–NH<sub>2</sub> (site 2) are listed in Table S1 (ESI†).

### 2.2 Force field and partial charge of atoms

In this work, Lennard-Jones (LJ) and Coulombic potentials were combined to calculate the interactions between adsorbates and MOF or among adsorbates, and the cross parameters of the Lennard-Jones potential were calculated by the Lorentz–Berthelot (LB) combined rules. Based on previous studies, we know that DREIDING<sup>19</sup> and UFF force fields<sup>20</sup> are usually used to calculate the adsorption properties of MOF on gases, and Yang *et al.*<sup>21</sup> validated that the DREIDING force field is more suitable for describing the adsorption of N<sub>2</sub> molecules on UiO-66. However, different structures correspond to different features, and the existing parameters cannot properly represent the interactions

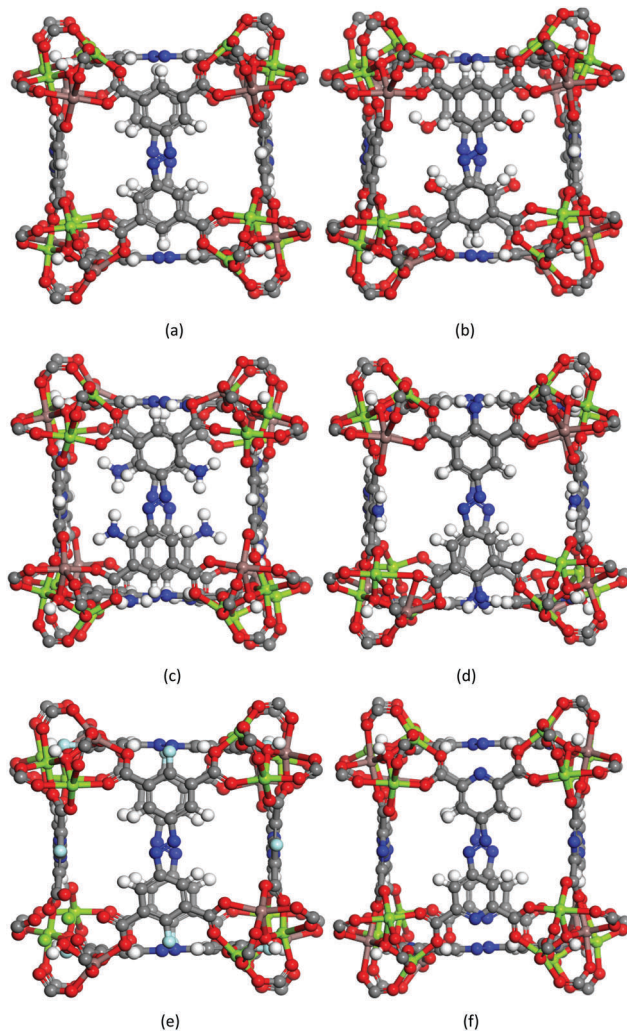


**Fig. 1** The structural sketches of CPM-200-In/Mg (a) and CPM-200-In/Mg-X (X = -OH (b), -NH<sub>2</sub> (site 1 (c), site 2 (d)), -F (e), -N (f)). Brown, fluorescent, gray, red, dark blue, baby blue and white balls denote In, Mg, C, O, N, F and H atoms, respectively.

**Table 1** Structural properties of CPM-200-In/Mg and CPM-200-In/Mg-X

Materials	$\rho_{\text{cryst}}^a$ (g cm <sup>-3</sup> )	$V_{\text{pore}}^a$ (cm <sup>3</sup> g <sup>-1</sup> )	$S_{\text{acc}}^b$ (Å <sup>2</sup> )
CPM-200-In/Mg	0.851	0.787	3040.70
-F	0.863	0.769	3214.23
-OH	0.909	0.735	3078.41
-N	0.855	0.785	2993.98
-NH <sub>2</sub> (site 1)	0.892	0.753	3090.68
-NH <sub>2</sub> (site 2)	0.879	0.757	3201.24

<sup>a</sup> Data were calculated by RASPA. <sup>b</sup> Data were calculated by Materials Studio.

between the gas molecules and the MOFs, as shown in Fig. 2, where the generic force field cannot describe the behavior of CO<sub>2</sub> on CPM-200-In/Mg very well at 273 or 298 K. Therefore, in accordance with the experiment, part of the force field parameters must be refined.

The parameters of the modified force field are shown in Table S2 (ESI†), while the potential parameters for most of the

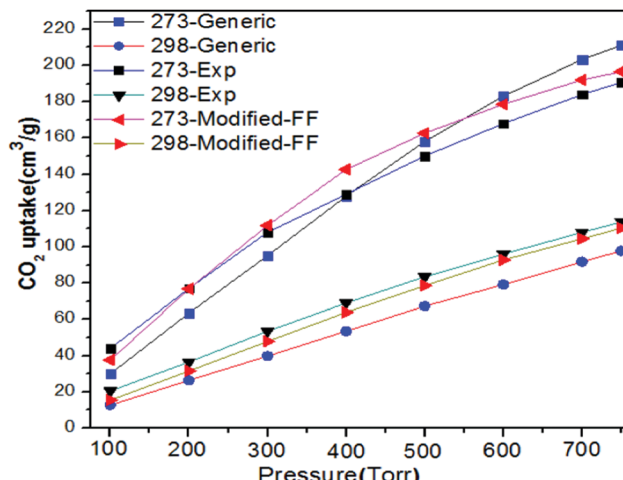


**Fig. 2** The experimental and simulated adsorption isotherms (with Generic and MFF respectively) of CO<sub>2</sub> in CPM-200-In/Mg at 273 K and 298 K, respectively.

guest molecules were obtained from the TraPPE force field<sup>22</sup> and are listed in Table S3 (ESI†). Compared with the generic force field, the modified force field can better describe the CO<sub>2</sub> adsorption behavior, as shown in Fig. 2. With the new modified force field (MFF), the adsorption behaviors of N<sub>2</sub>, H<sub>2</sub>, CH<sub>4</sub> and C<sub>2</sub>H<sub>2</sub> in CPM-200-In/Mg were found to be well in agreement with the experimental data, as shown in Fig. 3. In addition, the partial charges in MOFs were calculated at the DFT of the Perdew–Burke–Ernzerhof (PBE) exchange and correlation functional using the GAUSSIAN 09 program package<sup>23</sup> with cleaved clusters, as shown in Fig. 4. The electrostatic potential (ESP) charges obtained via the ChelpG method, which has been recognized as the most popular and reliable method for electrostatic charge calculation,<sup>24</sup> were used as the atomic partial charges. The electrostatic potential of CPM-200-In/Mg and the HOMO–LUMO gap of ligands were also calculated at the same level. For all the DFT calculations, the pseudo potential basis set of LANL2DZ was used for In and Mg atoms, while the 6-31+G(d) basis set including one diffuse and one polarization function on atoms heavier than helium was employed for the rest of the atoms. Note that the atomic van der Waals (VDW) radii for the framework elements used to fit the ESP charges were taken from the work of Santiago Alvarez.<sup>25</sup>

### 2.3 Simulation details

Grand-canonical Monte Carlo (GCMC) using the RASPA code<sup>26</sup> was employed to simulate the adsorption behavior of gases (HCHO, HCN, SO<sub>2</sub>, H<sub>2</sub>S, CH<sub>4</sub>, C<sub>2</sub>H<sub>4</sub>, C<sub>2</sub>H<sub>2</sub>, C<sub>2</sub>H<sub>6</sub>, C<sub>3</sub>H<sub>8</sub>, C<sub>2</sub>H<sub>3</sub>Cl, C<sub>2</sub>H<sub>2</sub>Cl<sub>2</sub>, CHCl<sub>3</sub> and CH<sub>2</sub>Cl<sub>2</sub>) as well as the selectivity of H<sub>2</sub>S (0.002)-CO<sub>2</sub> (0.263)-CH<sub>4</sub> (0.735) (mole fraction) and SO<sub>2</sub> (0.002)-CO<sub>2</sub> (0.198)-N<sub>2</sub> (0.8) (mole fraction) gas mixtures in CPM-200-In/Mg and CPM-200-In/Mg-X. The materials were modeled as rigid structures, ignoring the skeleton stretching and bending vibrations. All GCMC simulations were run for 100 000 equilibrium cycles, followed by 100 000 cycles for statistical data collection. Every cycle includes N steps corresponding

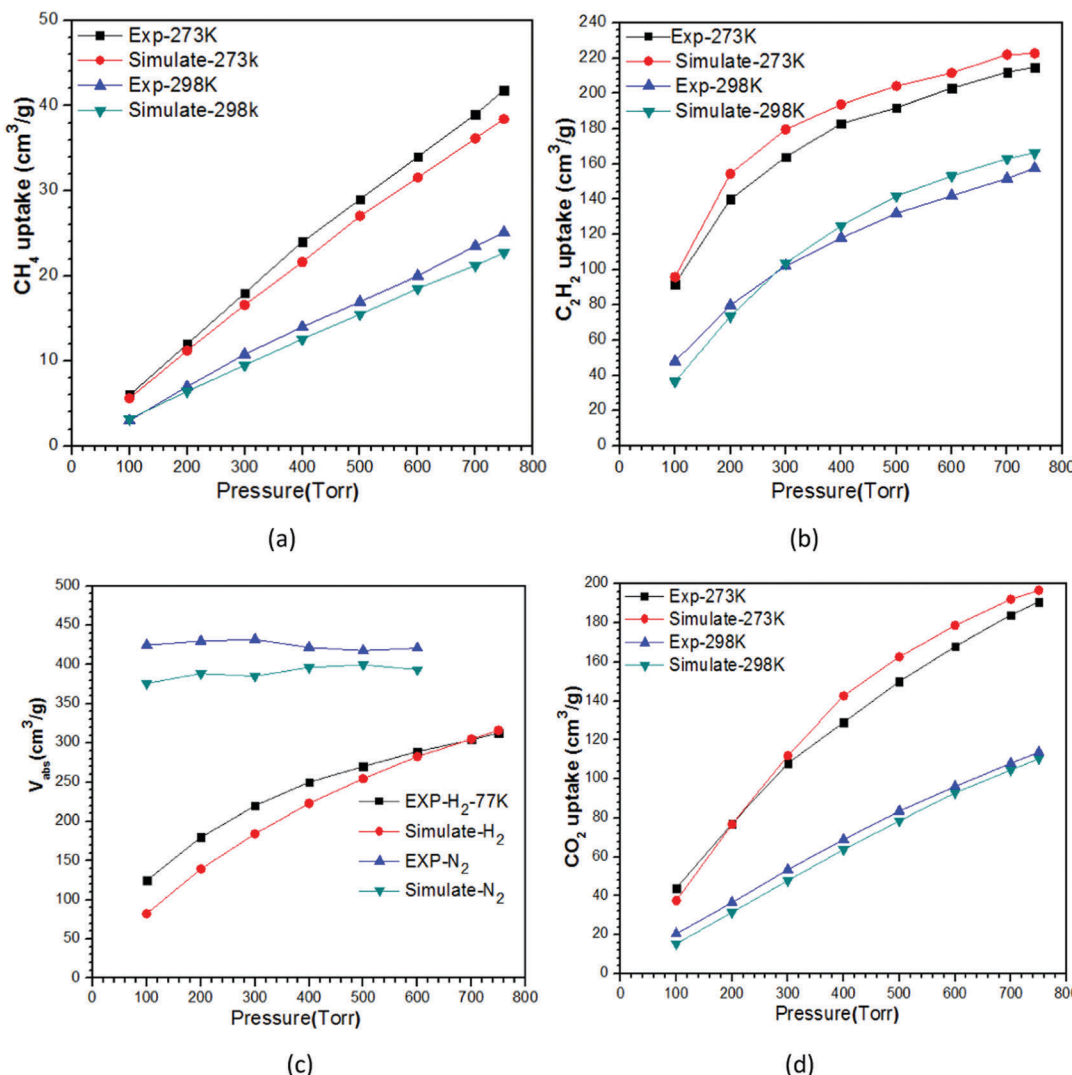


**Fig. 3** Experimental and simulated adsorption isotherms (with MFF) of  $\text{CH}_4$  (a),  $\text{C}_2\text{H}_2$  (b),  $\text{N}_2$  (c),  $\text{H}_2$  (d) and  $\text{CO}_2$  (e) in CPM-200-In/Mg at 273 K and 298 K, respectively.

to the number of the gas molecules in the system, and a minimum of 20 steps were used when the number of gas molecules was less than 20. Every GCMC step consists of five types of trial motions for gas molecules, namely insertion, rotation, translation, deletion and random reinsertion.

### 3. Results and discussion

In Section 3.1 we investigate the adsorption capacities of CPM-200-In/Mg for some harmful inorganic gases ( $\text{CO}_2$ ,  $\text{H}_2\text{S}$ ,  $\text{SO}_2$ ,  $\text{HCN}$ ,  $\text{NH}_3$ ,  $\text{NO}$  and  $\text{CO}$ ) and VOCs ( $\text{HCHO}$ ,  $\text{C}_2\text{H}_6$ ,  $\text{C}_3\text{H}_8$ ,  $\text{C}_2\text{H}_2$ ,  $\text{C}_2\text{H}_4$ ,  $\text{CH}_4$ ,  $\text{CHCl}_3$ ,  $\text{CH}_2\text{Cl}_2$ ,  $\text{C}_2\text{H}_3\text{Cl}$  and  $\text{C}_2\text{H}_2\text{Cl}_2$ ). In Section 3.2 we analyze the adsorption mechanism of CPM-200-In/Mg for  $\text{HCN}$ ,  $\text{HCHO}$  as well as the chlorine derivatives of  $\text{CH}_4$  and  $\text{C}_2\text{H}_4$ . In Section 3.3 we explore the selectivity of CPM-200-In/Mg for sulfide and carbide, and in the last Section of 3.4, we further investigate the adsorption capacity for  $\text{CO}_2$  and  $\text{HCHO}$  of CPM-200-In/Mg with functional groups ( $-\text{NH}_2$ ,  $-\text{OH}$ ,  $-\text{N}$ ,  $-\text{F}$ )

and selectivity to ternary mixture systems including natural gas and post-combustion flue gas.

#### 3.1 The adsorption capacities of CPM-200-In/Mg for low molecular weight gases

First of all, we explored the adsorption capacities of some inorganic gases ( $\text{CO}_2$ ,  $\text{H}_2\text{S}$ ,  $\text{SO}_2$ ,  $\text{HCN}$ ,  $\text{NH}_3$ ,  $\text{NO}$  and  $\text{CO}$ ) and VOCs ( $\text{HCHO}$ ,  $\text{C}_2\text{H}_6$ ,  $\text{C}_3\text{H}_8$ ,  $\text{C}_2\text{H}_2$ ,  $\text{C}_2\text{H}_4$ ,  $\text{CH}_4$ ,  $\text{CHCl}_3$ ,  $\text{CH}_2\text{Cl}_2$ ,  $\text{C}_2\text{H}_3\text{Cl}$  and  $\text{C}_2\text{H}_2\text{Cl}_2$ ) using MFF. From the plotted adsorption isotherms of VOCs and inorganic harmful gases on CPM-200-In/Mg at 298 K in Fig. 5, it is clear that CPM-200-In/Mg can effectively capture gases, particularly  $\text{HCHO}$  ( $270.34 \text{ cm}^3 \text{ g}^{-1}$  or  $0.39 \text{ g g}^{-1}$ , 298 K, 1 bar),  $\text{HCN}$  ( $279.16 \text{ cm}^3 \text{ g}^{-1}$ , 298 K, 0.8 bar) and  $\text{SO}_2$  ( $269.66 \text{ cm}^3 \text{ g}^{-1}$ , 298 K, 1 bar). Moreover, the adsorption capacities of CPM-200-In/Mg for  $\text{NO}$ ,  $\text{CO}$  and  $\text{CH}_4$  are very low, below  $25 \text{ cm}^3 \text{ g}^{-1}$ , while those for the other gases are as large as between  $100 \text{ cm}^3 \text{ g}^{-1}$  and  $170 \text{ cm}^3 \text{ g}^{-1}$  at normal temperature and pressure (NTP). It is worth noting that as the most effective

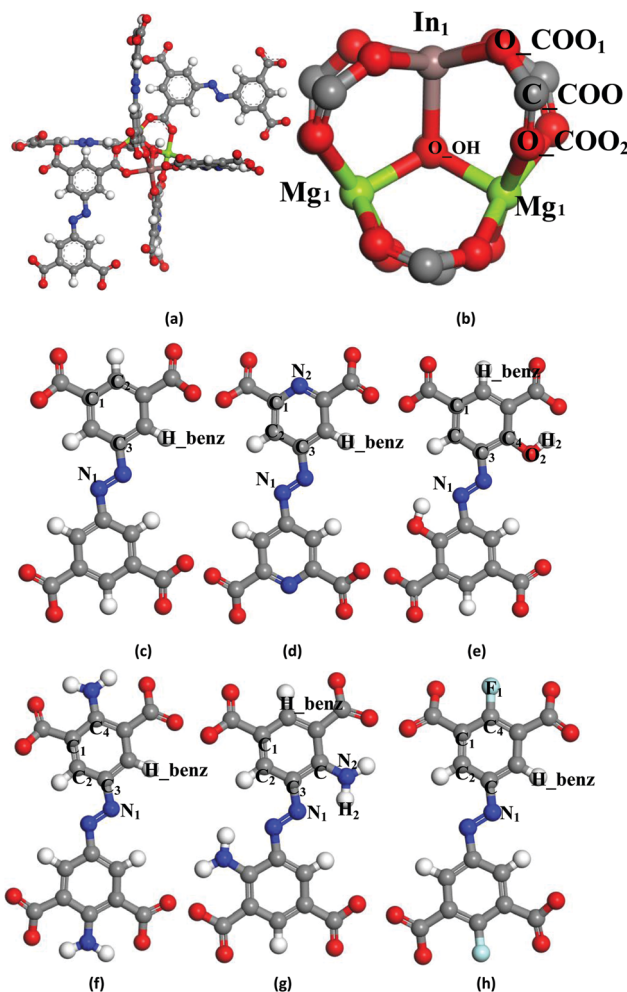


**Fig. 4** (a) Fragmented cluster model of MOFs for fitting charge, (b) metal cluster of MOFs, (c) ligand clusters of CPM-200-In/Mg and CPM-200-In/Mg-X (–N (d), –OH (e), –NH<sub>2</sub> (site 2, (f)), –NH<sub>2</sub> (site 1, (g)), –F (h)); brown, fluorescent, gray, red, dark blue, baby blue and white balls denote In, Mg, C, O, N, F and H atoms, respectively.

traditional adsorbent for HCHO (a common indoor pollutant), the adsorption capacity of activated carbon is just  $0.009\text{ g g}^{-1}$  at NTP. With the related application of MOFs as an adsorbent, the versatile mesoporous 438-MOF is one of the efficient adsorbents for HCHO, but with just  $0.22\text{ g g}^{-1}$  at NTP.<sup>27</sup> Therefore, CPM-200-In/Mg should be a more effective adsorbent for HCHO (up to  $0.39\text{ g g}^{-1}$  at NTP) than 438-MOF.

The adsorption character of CPM-200-In/Mg for gases is discussed in detail according to their adsorption isotherms as shown in Fig. 5. From Fig. 5(a–d), we can see that except for CH<sub>4</sub> and C<sub>2</sub>H<sub>4</sub>, the VOCs (HCHO, C<sub>2</sub>H<sub>6</sub>, C<sub>3</sub>H<sub>8</sub>, C<sub>2</sub>H<sub>2</sub>, CHCl<sub>3</sub>, CH<sub>2</sub>Cl<sub>2</sub>, C<sub>2</sub>H<sub>3</sub>Cl and C<sub>2</sub>H<sub>2</sub>Cl<sub>2</sub>) can be adsorbed by CPM-200-In/Mg more easily than inorganic gases (H<sub>2</sub>S, NH<sub>3</sub>, CO<sub>2</sub>, NO and CO) within 600 Torr; *i.e.*, CPM-200-In/Mg is capable of effectively capturing the VOCs in low pressure areas ( $\leq 1$  bar). For example, the adsorption capacities of CHCl<sub>3</sub> and C<sub>2</sub>H<sub>2</sub>Cl<sub>2</sub> as shown in Fig. 5(e) are close to saturation within 1000 Pa. Moreover, from the adsorption isotherms of CH<sub>4</sub>, C<sub>2</sub>H<sub>4</sub> and their derivatives including CHCl<sub>3</sub>, CH<sub>2</sub>Cl<sub>2</sub>, C<sub>2</sub>H<sub>3</sub>Cl and C<sub>2</sub>H<sub>2</sub>Cl<sub>2</sub>

on CPM-200-In/Mg as shown in Fig. 5(d), we can see that the adsorption capacities of chlorine derivatives are much higher than those of CH<sub>4</sub> and C<sub>2</sub>H<sub>4</sub> due to the strong electron withdrawing ability of the chlorine atom. Besides, the adsorption capacities of some inorganic gases, including SO<sub>2</sub>, H<sub>2</sub>S and CO<sub>2</sub>, as shown in Fig. 5(b and c), match well with their polarizability values, *i.e.*, SO<sub>2</sub> ( $26a_0^3$ )  $>$  H<sub>2</sub>S ( $25a_0^3$ )  $>$  CO<sub>2</sub> ( $18a_0^3$ ).<sup>28</sup> In addition, from Fig. 5(f and g), we can see that positive charges of CPM-200-In/Mg are mainly distributed on metal atoms and the carbon atoms of carboxylic acid groups, while negative charges are mainly distributed on oxygen and nitrogen atoms. The electrostatic potential distribution of the CPM-200-In/Mg metal center ranges from  $-1$  a.u. to  $0.7$  a.u. and that of the CPM-200-In/Mg organic ligand is from  $-0.05$  a.u. to  $0.05$  a.u.; *i.e.*, compared with an organic ligand, the metal center has a larger electrostatic potential gradient and electrostatic potential. Thus, the adsorbate tends to be adsorbed at the metal center. From the snapshots of C<sub>2</sub>H<sub>4</sub>, CH<sub>4</sub> and their derivatives in CPM-200-In/Mg plotted in Fig. S1 (ESI†), it is shown that adsorbate molecules are first adsorbed close to the metal center in the low pressure area and are then gradually adsorbed in porous channels, accompanied by the pressure increase. Thus, we can reasonably infer that the molecules with large polarizability will be helpful for adsorption on CPM-200-In/Mg.

### 3.2 The adsorption mechanism of CPM-200-In/Mg for low molecular weight gases

In this section, we focus on the adsorption mechanism of CPM-200-In/Mg for some harmful gases with high capacities. From Fig. 5(a–d), we can see that HCN and HCHO have the largest adsorption capacities on CPM-200-In/Mg among the inorganic harmful gases and VOCs, respectively. Moreover, the adsorption capacities of CPM-200-In/Mg for chlorine derivatives are much larger than those for CH<sub>4</sub> and C<sub>2</sub>H<sub>4</sub>. Taking CHCl<sub>3</sub> as an example, its adsorption capacity is about 38 times that of CH<sub>4</sub> at 298 K and 100 Torr. In the following, we will investigate the mechanism of CPM-200-In/Mg for those gas molecules with high adsorption capacities from two aspects, namely, radial distribution functions (RDF,  $g(r)$ ) and interaction energy.

First, we will discuss the adsorption mechanism from the perspective of RDF between adsorbed molecules and specific framework atoms as shown in Fig. S2 (ESI†).

For the inorganic gas molecules, comparing the RDF of HCN with that of NH<sub>3</sub> in Fig. S2(a and b) (ESI†), we can see that NH<sub>3</sub> acting as a strong electron donor has a strong base-acid interaction with the carboxylic acid groups as shown in Fig. S2(b<sub>3</sub>) (ESI†), and from Fig. S2(a<sub>3</sub> and b<sub>3</sub>) (ESI†) we can see that NH<sub>3</sub> can be better adsorbed by CPM-200-In/Mg at carboxylic acid groups than HCN. Although HCN has a strong interaction with a metal center, it is still slightly weaker than that of NH<sub>3</sub>, as shown in Fig. S2(a<sub>1</sub> and b<sub>1</sub>) (ESI†). However, the NH<sub>3</sub> molecule has only one action site (N action site), while the HCN molecule has three (H, C and N, with N being the strongest action site). From Fig. S2(a<sub>2</sub>–a<sub>4</sub>) (ESI†), it is shown that HCN with three action sites is not only a proton donor but also an acceptor; for example, the C and H atoms of HCN as electron deficient atoms

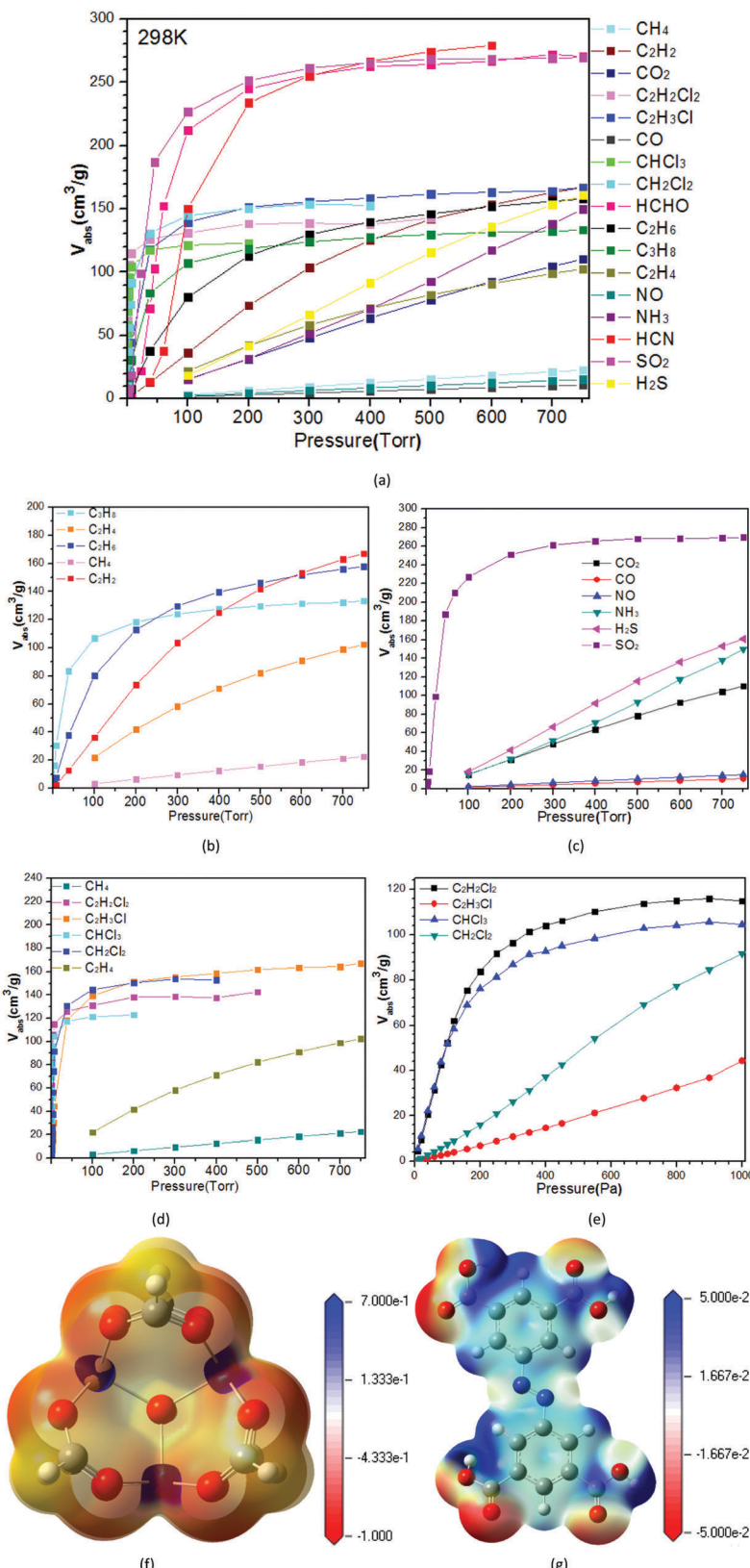


**Fig. 5** (a) Simulated adsorption isotherms of gases we investigated for CPM-200-In/Mg at 298 K. (b) Simulated adsorption isotherms of  $\text{CH}_4$ ,  $\text{C}_2\text{H}_6$ ,  $\text{C}_3\text{H}_8$  and  $\text{C}_2\text{H}_4$  for CPM-200-In/Mg at 298 K. (c) Simulated adsorption isotherms of inorganic molecules for CPM-200-In/Mg at 298 K. (d) and (e) Simulated adsorption isotherms of methane, ethene and their chlorine substituents for CPM-200-In/Mg. (f) and (g) The electrostatic potential distribution of the CPM-200-In/Mg metal center and organic ligand.

can interact with the O and N atoms of the organic ligand to some extent. Therefore, HCN has a much stronger interaction with the organic ligand than NH<sub>3</sub>. Furthermore, from Fig. 5(a), we know that acidic HCN molecules as proton donors are more likely to be adsorbed by CPM-200-In/Mg, though NH<sub>3</sub> has a stronger base-acid interaction with carboxylic acid groups.

For the organic gas molecules, comparing the RDFs of HCHO with C<sub>2</sub>H<sub>4</sub>, CH<sub>4</sub> and their chlorine derivatives as shown in Fig. S2c-i (ESI†), we can see that pronounced peaks in  $g(r)$ , whether between HCHO molecules and metal central atoms or carboxylic acid groups, are observed at  $r = 2.5\text{--}4.5 \text{ \AA}$ , particularly for the O atom of HCHO with magnesium at 2.75 Å. On the contrary, there are just weak peaks at  $r = 2.5\text{--}4.5 \text{ \AA}$  for the remaining VOCs. Therefore, HCHO has a greater probability to be adsorbed by CPM-200-In/Mg than other VOCs.

It is important to compare the RDFs of C<sub>2</sub>H<sub>4</sub>, CH<sub>4</sub> and their chlorine derivatives. We find that all of them have very weak interactions with a metal center, which is different from HCHO, and the strength of their pair interactions between action sites and special framework atoms is slightly different. In addition, compared with C<sub>2</sub>H<sub>4</sub> and CH<sub>4</sub>, their chlorine derivatives have more interaction pairs and their proton donor abilities are strengthened; namely, the H and C atoms close to the Cl atom of chlorine derivatives have more positive charges. From the radial distribution of H atoms with framework atoms as shown in Fig. S2(f-i) (ESI†), we can see that the average distribution distances between H atoms and framework atoms (except for metal elements) are larger than the sum of their van der Waals radii ( $r_C = 1.77 \text{ \AA}$ ,  $r_O = 1.50 \text{ \AA}$ ,  $r_N = 1.66 \text{ \AA}$ ,  $r_H = 1.2 \text{ \AA}$ ); thus the interactions between H atoms and framework atoms are considered as weak electrostatic interactions. In addition, from the snapshots of C<sub>2</sub>H<sub>4</sub>, CH<sub>4</sub> and their chlorine derivatives as shown in Fig. S1 (ESI†), it was found that compared to CH<sub>4</sub> and C<sub>2</sub>H<sub>4</sub>, the Cl and H atoms of chlorine derivatives will be quickly adsorbed on the framework, which proves indirectly the importance of polarity in adsorption. From Fig. S2(f<sub>1</sub>, g<sub>1</sub>, h<sub>1</sub> and i<sub>1</sub>) (ESI†), it is surprisingly found that the average distribution distances between main-group metal atoms and Cl atoms of chlorine derivatives are all within 4 Å, which is less than the sum of their van der Waals radii ( $r_{In} = 2.43 \text{ \AA}$ ,  $r_{Mg} = 2.51 \text{ \AA}$ ,  $r_{Cl} = 1.82 \text{ \AA}$ ); *i.e.*, there exist secondary bonds (weak halogen bonds). This is one of the reasons for the chlorine derivatives (C<sub>2</sub>H<sub>3</sub>Cl, C<sub>2</sub>H<sub>2</sub>Cl<sub>2</sub>, CH<sub>2</sub>Cl<sub>2</sub> and CHCl<sub>3</sub>) to have higher adsorption capacities than CH<sub>4</sub> and C<sub>2</sub>H<sub>4</sub>. However, with the increase in pressure, as shown in Fig. 5(a), the adsorption capacities of C<sub>2</sub>H<sub>3</sub>Cl (29.30 bohr<sup>3</sup>) and CH<sub>2</sub>Cl<sub>2</sub> (29.07 bohr<sup>3</sup>) in CPM-200-In/Mg would surpass those of CHCl<sub>3</sub> (39.06 bohr<sup>3</sup>) and C<sub>2</sub>H<sub>2</sub>Cl<sub>2</sub> (39.21 bohr<sup>3</sup>); note that the values in parentheses are the polarizability values. Thus, polarizability is not the only influencing factor. From Fig. S2(f<sub>1</sub>, g<sub>1</sub>, h<sub>1</sub> and i<sub>1</sub>) (ESI†), it is shown that C<sub>2</sub>H<sub>3</sub>Cl and CH<sub>2</sub>Cl<sub>2</sub> can form stronger halogen bonds than C<sub>2</sub>H<sub>2</sub>Cl<sub>2</sub> and CHCl<sub>3</sub>. Particularly, there is an obvious peak at 4 Å for C<sub>2</sub>H<sub>3</sub>Cl, which rationalizes why the adsorption capacities of C<sub>2</sub>H<sub>3</sub>Cl and CH<sub>2</sub>Cl<sub>2</sub> can surpass those of C<sub>2</sub>H<sub>2</sub>Cl<sub>2</sub> and CHCl<sub>3</sub> in relatively high pressure, as shown in Fig. 5(a); therefore, compared with CH<sub>4</sub> and C<sub>2</sub>H<sub>4</sub>, their chlorine derivatives have more

action sites (proton donors), greater polarity and halogen bonds, which strengthen their interaction with the framework.

We then explored the adsorption mechanism of organic CH<sub>4</sub>, C<sub>2</sub>H<sub>4</sub> and their derivatives in CPM-200-In/Mg from the perspective of interaction energy. From Fig. S3 (ESI†), we find that the isosteric heat of chlorine derivatives interacting with MOF is generally larger than that of CH<sub>4</sub> and C<sub>2</sub>H<sub>4</sub> in the order CHCl<sub>3</sub> ≥ C<sub>2</sub>H<sub>2</sub>Cl<sub>2</sub> > CH<sub>2</sub>Cl<sub>2</sub> > C<sub>2</sub>H<sub>3</sub>Cl > C<sub>2</sub>H<sub>2</sub> > C<sub>2</sub>H<sub>4</sub> > CH<sub>4</sub>. From Fig. 5(e), we know that the order of isosteric heat of chlorine derivatives basically agrees with that of their adsorption capacities within 1000 Pa. From the VDW and Coulomb interactions between MOF and CH<sub>4</sub>, C<sub>2</sub>H<sub>4</sub> as well as their derivatives plotted in Fig. S4 (ESI†), it is shown that CH<sub>4</sub> and C<sub>2</sub>H<sub>4</sub> interact with CPM-200-In/Mg only through very weak VDW interactions (Fig. S4a (ESI†)). However, when the hydrogen atoms of CH<sub>4</sub> and C<sub>2</sub>H<sub>4</sub> are replaced by chlorine atoms (strong electron acceptors), their VDW (Fig. S4b (ESI†)) and Coulomb interactions (Fig. S4c (ESI†)) with the framework are enhanced greatly, particularly for CHCl<sub>3</sub> and C<sub>2</sub>H<sub>2</sub>Cl<sub>2</sub>. For example, the VDW interaction between CHCl<sub>3</sub> and MOF reached 258 kJ per uc at 50 Pa, compared to that between CH<sub>4</sub> and the framework at just 70 kJ per uc at 700 Torr. Thus, chlorine substitution can enhance their isosteric heat leading to high uptake in low pressure areas. By analyzing the RDF and the interaction energy between adsorbates and MOF, we can confirm that the large adsorption capacities of HCN and HCHO in the framework result from the strong interaction between adsorbates and metal centers. On the other hand, the high adsorption capacities of chlorine derivatives in the framework could be due to the existence of halogen-bonding or strong electrostatic and VDW interactions, while C<sub>2</sub>H<sub>4</sub> and CH<sub>4</sub> molecules just interact with CPM-200-In/Mg by VDW interaction.

### 3.3 Adsorption selectivity of CPM-200-In/Mg for sulfide and carbide

As we all know, the existence of sulfide and carbide in natural gas or flue gas is harmful to our environment. Thus, we also explored the adsorption selectivity of CPM-200-In/Mg in two ternary mixture systems, namely natural gas and post-combustion flue gas, with corresponding proportions of components: H<sub>2</sub>S ( $y_{H_2S} = 0.002$ )–CO<sub>2</sub> ( $y_{CO_2} = 0.263$ )–CH<sub>4</sub> ( $y_{CH_4} = 0.735$ ) and SO<sub>2</sub> ( $y_{SO_2} = 0.002$ )–CO<sub>2</sub> ( $y_{CO_2} = 0.198$ )–N<sub>2</sub> ( $y_{N_2} = 0.198$ ). The initial contents of H<sub>2</sub>S and SO<sub>2</sub> are derived from the literature,<sup>29</sup> based on the actual contents of natural gas and post-combustion flue gas. The selectivity is calculated by the following formula:

$$S_{ij} = \frac{x_i/x_j}{y_i/y_j}; \quad S_s = \frac{x_s(1-y_s)}{y_s(1-x_s)}; \quad S_{sc} = \frac{(x_s + x_{CO_2})(1 - y_s - y_{CO_2})}{(y_s + y_{CO_2})(1 - x_s - x_{CO_2})},$$

where  $S_{ij}$  refers to the selectivity of the first component  $i$  over the second component  $j$ ,  $S_s$  denotes the desulfurization ability alone,  $S_{sc}$  denotes the desulfurization and decarburetion abilities simultaneously, the subscript s means the sulfide gas of H<sub>2</sub>S or SO<sub>2</sub>, and  $x$  and  $y$  denote the molar fractions of species in the adsorbed and bulk phases, respectively. The simulated adsorption results include the adsorption of single components

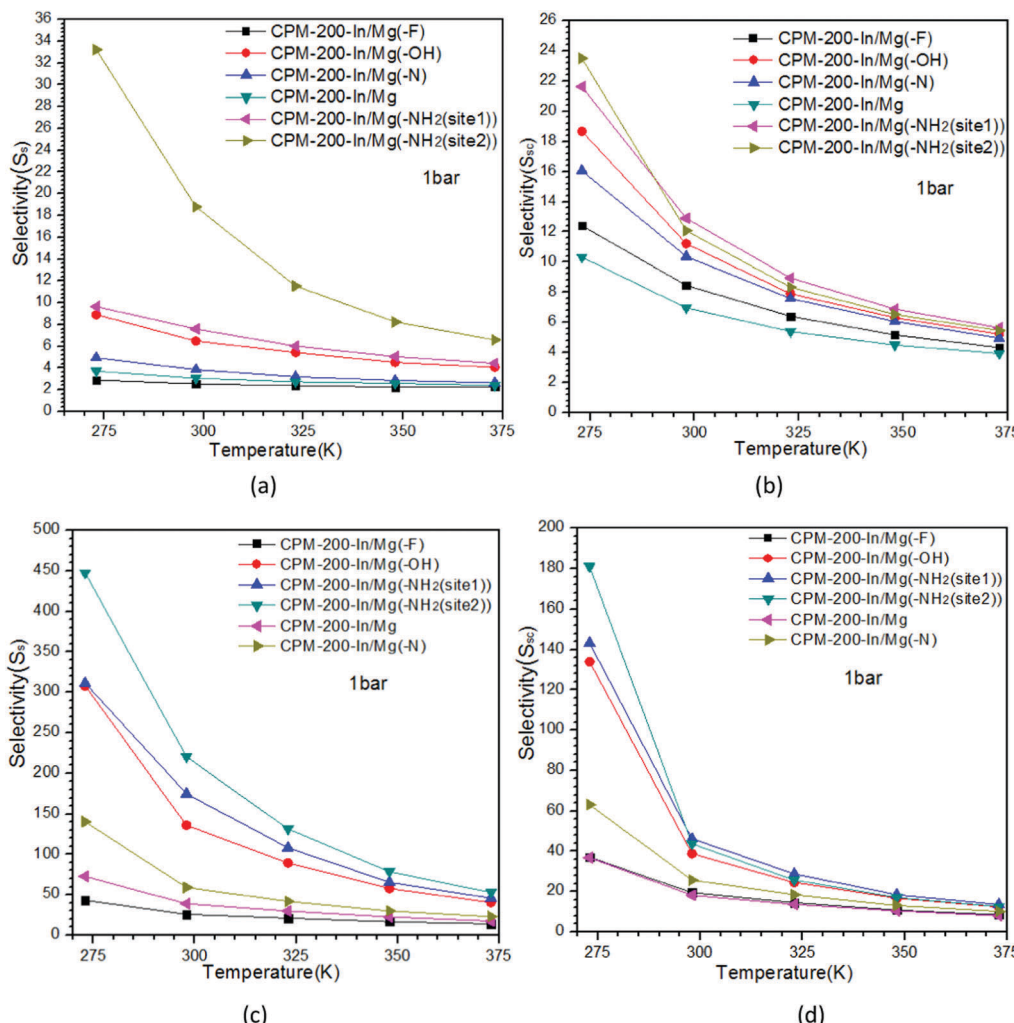


**Fig. 6** The effects of temperature on the gas selectivity of materials in  $\text{CO}_2\text{-H}_2\text{S}\text{-CH}_4$  (a and b) and  $\text{CO}_2\text{-SO}_2\text{-N}_2$  (c and d) ternary mixtures systems at 1 bar.

and the separation of multi-components as shown in Fig. 6 and Fig. S5–S7 (ESI†).

Next, we investigated the separation ability of CPM-200-In/Mg in the natural gas ternary mixture system ( $\text{H}_2\text{S}\text{-CO}_2\text{-CH}_4$ ). From Section 3.2, we know that the adsorption behavior of  $\text{CH}_4$  molecules on CPM-200-In/Mg is only dominated by VDW interaction. However, for the polar molecule  $\text{H}_2\text{S}$ , in addition to VDW interactions, it can interact with MOF by Coulombic electrostatic forces and hydrogen-bonding interactions. Therefore, compared to the nonpolar and low polarizability  $\text{CH}_4$  molecule,  $\text{H}_2\text{S}$  has much higher adsorption capacity in CPM-200-In/Mg. From Fig. S5 and S7 (ESI†), it is found that CPM-200-In/Mg can separate  $\text{H}_2\text{S}$  by  $S_s = 3.0$  at NTP, but its ability to remove  $\text{H}_2\text{S}$  from the  $\text{H}_2\text{S}\text{-CO}_2\text{-CH}_4$  mixture ( $S_s = 4.5$ ) is much weaker than that of the MOF-74 series ( $S_s \geq 10$ )<sup>29</sup> at 303 K and 4 MPa. However, its ability to remove  $\text{CO}_2$  and  $\text{H}_2\text{S}$  simultaneously ( $S_{sc} = 11$ ) is better than that of the MOF-74 series ( $< 10$ ).<sup>29</sup> Besides, when the pressure increases ( $\leq 1$  bar),  $S_{sc}$  increases slightly, while  $S_s$  remains constant.

As for the  $\text{SO}_2\text{-CO}_2\text{-N}_2$  ternary mixture, the abilities for desulfurization ( $S_s$ ) or desulfurization and decarburization

( $S_{sc}$ ) simultaneously for CPM-200-In/Mg are  $S_s = 57$  and  $S_{sc} = 40$ , respectively, at 303 K and 4 MPa. As is known, MOF-74-Zn has the largest selectivity for sulfide among the MOF-74 series,<sup>29</sup> with  $S_s = 200$  and  $S_{sc} = 80$ , which are much larger than those of CPM-200-In/Mg. Thus, in the following section, we will try to introduce some functional groups to CPM-200-In/Mg to increase the gas adsorption, desulfurization and decarburization abilities.

### 3.4 Adsorption capacity and selectivity of CPM-200-In/Mg with functional groups

**3.4.1 The effects of  $-\text{NH}_2$ ,  $-\text{OH}$ ,  $-\text{N}$  and  $-\text{F}$  functional groups on gas adsorption and separation.** From Section 3.1, we know that gas molecules with larger polarizability will have higher capacities in CPM-200-In/Mg, and most of the harmful gases we investigated are acidic molecules (electron deficient molecules). Therefore, we tried to introduce basic groups including  $-\text{NH}_2$ ,  $-\text{OH}$ ,  $-\text{N}$ , and also  $-\text{F}$  into CPM-200-In/Mg to explore their effects on the gas adsorption and separation abilities.

First, by introducing  $-\text{NH}_2$ ,  $-\text{OH}$  and  $-\text{N}$  basic groups to CPM-200-In/Mg, we investigated the effects on gas adsorption

capacity. To the best of our knowledge, only the following six MOFs have slightly higher CO<sub>2</sub> gravimetric uptake, including traditional homometallic or heterometallic MOFs, *i.e.*, Mg-MOF-74<sup>13</sup> (228 cm<sup>3</sup> g<sup>-1</sup>), Cu-TDPAT<sup>30</sup> (227 cm<sup>3</sup> g<sup>-1</sup>), Cu-TPBTM<sup>31</sup> (216 cm<sup>3</sup> g<sup>-1</sup>), CPM-200-Fe/Mg (207 cm<sup>3</sup> g<sup>-1</sup>), NJU-Bai21<sup>32</sup> (206 cm<sup>3</sup> g<sup>-1</sup>) and NbO-Pb-1<sup>33</sup> (201 cm<sup>3</sup> g<sup>-1</sup>) at 273 K and 1 bar. Comparing the absorption capacity of CO<sub>2</sub> of the above-mentioned MOFs with modified MOFs at 273 K and 1 bar, as shown in Fig. S6(a) (ESI†), the sequence is as follows: -NH<sub>2</sub> (site 2, 245 cm<sup>3</sup> g<sup>-1</sup>) > MOF-74-Mg (228 cm<sup>3</sup> g<sup>-1</sup>) > Cu-TDPAT (227 cm<sup>3</sup> g<sup>-1</sup>) > -N (222 cm<sup>3</sup> g<sup>-1</sup>) > -OH (218 cm<sup>3</sup> g<sup>-1</sup>) > -NH<sub>2</sub> (site 1, 217 cm<sup>3</sup> g<sup>-1</sup>) > Cu-TPBTM (216 cm<sup>3</sup> g<sup>-1</sup>) > CPM-200-Fe/Mg (207 cm<sup>3</sup> g<sup>-1</sup>) > NJU-Bai21 (206 cm<sup>3</sup> g<sup>-1</sup>) > NbO-Pb-1 (201 cm<sup>3</sup> g<sup>-1</sup>) > -F (193 cm<sup>3</sup> g<sup>-1</sup>) > CPM-200-In/Mg (191 cm<sup>3</sup> g<sup>-1</sup>). Therefore, the CPM-200-In/Mg with -NH<sub>2</sub> (site 2) basic group has the largest adsorption capacity (245 cm<sup>3</sup> g<sup>-1</sup>) for CO<sub>2</sub>, which is even larger than that of MOF-74-Mg (228 cm<sup>3</sup> g<sup>-1</sup>, 1 bar, 273 K). Furthermore, the adsorption capacity order of CPM-200-In/Mg and CPM-200-In/Mg-X for HCHO, as shown in Fig. S6(b) (ESI†), is as follows: -NH<sub>2</sub> (site 2, 0.410 g g<sup>-1</sup>) > -N (0.400 g g<sup>-1</sup>) > -OH (0.399 g g<sup>-1</sup>) > -NH<sub>2</sub> (site 1, 0.396 g g<sup>-1</sup>) > -F (0.387 g g<sup>-1</sup>) > CPM-200-In/Mg (0.386 g g<sup>-1</sup>) > 438-MOF (0.22 g g<sup>-1</sup>) > active carbon (0.009 g g<sup>-1</sup>). From Fig. S6(b) (ESI†), it is shown that the introduction of basic groups can increase the adsorption capacity of MOFs for HCHO to some extent. For example, the adsorption capacity of CPM-200-In/Mg-NH<sub>2</sub> (site 2) for HCHO increased by 6% to 0.41 g g<sup>-1</sup>, compared to the original, which is almost twice that of 438-MOF and near 45 times that in active carbon.

It is important to interpret why basic group functionalized CPM-200-In/Mg has larger adsorption capacity. It was found that the -NH<sub>2</sub> group acting as an electron donor and -OH group acting as a proton acceptor can enhance the adsorption of the acid molecules in MOFs, such as H<sub>2</sub>S and CO<sub>2</sub>, as indicated by Loming Hamon, Daejin Kim, Zhiping Chen and Ziqi Tian works.<sup>34–37</sup> At the same time, the intramolecular hydrogen bonds created by inserted -NH<sub>2</sub> as well as -OH groups enhance the delocalization of the HOMO and thus lower the organic ligand HOMO-LUMO gaps of MOFs, which were calculated as shown in Table 2: source-ligand (4.297 eV) > ligand-F (4.261 eV) > pyridyl (4.008 eV) > ligand-OH (3.771 eV) > ligand-NH<sub>2</sub> (site 2, 3.682 eV) > ligand-NH<sub>2</sub> (site 1, 3.287 eV). Note that the -NH<sub>2</sub> group decreases the HOMO-LUMO gap the most, which is in accordance with the strongest gas adsorption and separation abilities among the functionalized MOFs, as shown in Fig. 6 and Fig. S5, S7 (ESI†). It is known that the smaller HOMO-LUMO gap has higher chemical activity,<sup>38</sup> which is favorable for the

interaction with molecular orbitals (MOs) of adsorbates.<sup>34–36</sup> Therefore, the small HOMO-LUMO gap should be responsible for the large adsorption capacities of CPM-200-In/Mg-NH<sub>2</sub> for CO<sub>2</sub> and HCHO. In addition, when the -NH<sub>2</sub> group replaces the H atom at site 2, the framework has much stronger intramolecular hydrogen bonds than at site 1, which is beneficial for the adsorption for acid molecules (CO<sub>2</sub> and HCHO) in CPM-200-In/Mg, as shown in Fig. S6(a and b) (ESI†). Compared with CPM-200-In/Mg, the mono-component adsorption capacities of CPM-200-In/Mg-NH<sub>2</sub> for CH<sub>4</sub> and N<sub>2</sub>, as the main components of natural gas and postcombustion flue gas, just change slightly as shown in Fig. S6(c and d) (ESI†); therefore, the CPM-200-In/Mg-NH<sub>2</sub> (site 2) may have excellent separation abilities for harmful gases. In addition, the polarity and alkalinity (N atom has a lone pair electron) of organic ligands are both improved after replacing benzene ring with the pyridyl group (-N); thus, CPM-200-In/Mg-N is helpful for the adsorption of those acidic molecules and enhances the separation of the sulfide and carbide in natural gas and post-combustion flue gas.

After the analysis of the adsorption capacities of CPM-200-In/Mg functionalized with basic groups, it was of interest to explore the selectivity of CPM-200-In/Mg in natural gas (H<sub>2</sub>S-CO<sub>2</sub>-CH<sub>4</sub>) and post-combustion flue gas (SO<sub>2</sub>-CO<sub>2</sub>-N<sub>2</sub>) mixtures in detail. From the work of Zhai *et al.*<sup>13</sup> and the present work, it was found that CPM-200-In/Mg has very poor separation ability for sulfide and carbide from post-combustion flue gas, although it has an excellent adsorption performance on CO<sub>2</sub>. Note that after the introduction of basic groups on the organic ligand, it is surprising that the adsorption ability of CPM-200-In/Mg for CO<sub>2</sub> is promoted to another level even beyond that of MOF-74-Mg. Therefore, we would like to find out whether the CPM-200-In/Mg with functional groups on organic ligands can be a great material for separating the sulfide and carbide from post-combustion flue gas and natural gas. From Fig. S5 (ESI†), it is shown that on functionalization with basic groups, the S<sub>s</sub> and S<sub>sc</sub> of CPM-200-In/Mg in ternary mixture systems are greatly enhanced at 298 K and low pressure ( $\leq 1$  bar). Specifically, the introduction of the -NH<sub>2</sub> group (site 1 or site 2) can enhance the abilities of S<sub>s</sub> and S<sub>sc</sub> the most. Note that S<sub>s</sub> of CPM-200-In/Mg-NH<sub>2</sub> (site 2) is six times the original and S<sub>sc</sub> is nearly three times the original at 298 K and 1 bar. Moreover, for the H<sub>2</sub>S-CO<sub>2</sub>-CH<sub>4</sub> ternary mixture, the abilities for desulfurization (S<sub>s</sub> = 24) and removing CO<sub>2</sub> and H<sub>2</sub>S simultaneously (S<sub>sc</sub> = 24) for CPM-200-In/Mg-NH<sub>2</sub> (site 2) have surpassed the MOF-74 series (S<sub>s</sub> < 20 and S<sub>sc</sub> < 10)<sup>29</sup> at 303 K and 4 MPa. As for the SO<sub>2</sub>-CO<sub>2</sub>-N<sub>2</sub> ternary mixture, owing to the higher polarity of SO<sub>2</sub>, the corresponding S<sub>s</sub> and S<sub>sc</sub> are much larger compared with those of H<sub>2</sub>S-CO<sub>2</sub>-CH<sub>4</sub> system at 298 K and low pressure area ( $\leq 1$  bar) as shown in Fig. S5 (ESI†). It is surprising that at 303 K and 4 MPa, the desulfurization ability (S<sub>s</sub>) of CPM-200-In/Mg-NH<sub>2</sub> (site 2) is increased from 57 to 190, which is comparable with that of the MOF-74 (S<sub>s</sub> ≤ 200)<sup>29</sup> series, and its simultaneous desulfurization and decarbureation ability (S<sub>sc</sub> ≤ 99) has surpassed that of the MOF-74 (S<sub>sc</sub> < 80)<sup>29</sup> series.

Second, with the introduction of -F, we focused on the effects on gas adsorption and selectivity of CPM-200-In/Mg. Combining

Table 2 HOMO-LUMO gaps of organic ligands

Adsorption site	HOMO/eV	LUMO/eV	LUMO-HOMO gap/eV
Source ligand	-7.459	-3.161	4.298
Ligand-F	-7.272	-3.010	4.262
Pyridyl	-7.942	-3.934	4.008
Ligand-OH	-6.977	-3.204	3.773
Ligand-NH <sub>2</sub> (site 2)	-5.793	-2.113	3.680
Ligand-NH <sub>2</sub> (site 1)	-6.278	-2.991	3.287

Table 1 and Fig. S6(a), (ESI†), we can see that compared with the other functional groups, the introduction of -F can best increase the accessible surface area from 3040.70 to 3214.23 Å<sup>2</sup>. However, contrary to the introduction of basic groups that can greatly increase the framework adsorption abilities whether for CO<sub>2</sub> at 273 K and 1 bar or for HCHO at NTP, the introduction of -F almost does not change the adsorption capacities to gas. This is to say, the increased surface area cannot strengthen its gas adsorption capacity, because the -F group weakens the adsorption interaction between CPM-200-In/Mg and acidic molecules including CO<sub>2</sub> and HCHO by lowering the electron density of the benzene ring. At the same time, the desulfurization ability of CPM-200-In/Mg-F in those two ternary mixtures is decreased in both. However, compared to its original counterpart, its  $S_{sc}$  in those two mixtures are both improved with the  $S_{sc}$  isothermal curves both being above those of CPM-200-In/Mg, as plotted in Fig. S5(b and d) (ESI†). From the mono-component adsorption isotherms of CO<sub>2</sub>, H<sub>2</sub>S, SO<sub>2</sub>, N<sub>2</sub> and CH<sub>4</sub> in MOFs as shown in Fig. S6(c and d) (ESI†), we find that the introduction of the -F group will decrease the adsorption capacity by 40 cm<sup>3</sup> g<sup>-1</sup> (from 161 cm<sup>3</sup> g<sup>-1</sup> to 121 cm<sup>3</sup> g<sup>-1</sup>) for H<sub>2</sub>S and just 14 cm<sup>3</sup> g<sup>-1</sup> for CO<sub>2</sub> at 1 bar, which could be attributed to the larger quadrupole moment, linear configuration (low steric effect) and large content of CO<sub>2</sub> near 20% in mixture systems (far exceeding the 0.2% content of sulfide in mixture systems). In addition, it is known that the ability of CPM-200-In/Mg with the basic group in adsorbing sulfide greatly exceeds that of CO<sub>2</sub>, which is mainly attributed to the stronger acid-basic interaction. However, this advantage of sulfide will no longer exist when CPM-200-In/Mg is modified with the -F group, accompanied by CO<sub>2</sub> capacity having little change, as plotted in Fig. S6(c and d) (ESI†). Therefore, compared to the original MOF, the -F group can greatly improve the adsorption competitiveness of CO<sub>2</sub> to sulfide as plotted in Fig. 6 and Fig. S7 (ESI†). Similarly, Chen *et al.*<sup>39</sup> also reported that it is possible to greatly improve the selectivity between C<sub>2</sub>H<sub>2</sub> and CO<sub>2</sub> with modified ligands, because the adsorption ability to C<sub>2</sub>H<sub>2</sub> is highly improved while that of CO<sub>2</sub> has a minute change. Thus, the introduction of -F is beneficial to the separation of CO<sub>2</sub> from natural gas and post-combustion flue gas mixture systems.

It should be noted that the introduction of basic groups of -NH<sub>2</sub>, -OH, -N and polarity group of -F would decrease the framework's pore volume as shown in Table 1. It is well known that the presence of functional groups may change the pore size, steric space, polarity and the hydrophilicity of materials, and larger pore volume and surface area are always thought to be in favor of gas adsorption. From Fig. S6(e) (ESI†), we can see that the pore size distributions (PSD) of CPM-200-In/Mg and functionalized CPM-200-In/Mg-X are mainly between 7 Å to 8.5 Å. Therefore, we can draw the conclusion that the pore size, pore volume and surface area are not the dominant factors for the gas adsorption and separation abilities of CPM-200-In/Mg with the introduction of functional groups in our work.

The acid-base interaction, hydrogen bond and electrostatic interaction are the main mechanisms for gas adsorption and separation of the title materials. The introduction of -NH<sub>2</sub>,

-OH and -N basic functional groups is beneficial for enhancing the framework's adsorption abilities for CO<sub>2</sub> and HCHO as well as desulfurization and decarburization abilities, while the introduction of the -F polarity group favors the CO<sub>2</sub> separation in natural gas and post-combustion flue gas.

**3.4.2 The effects of pressure and temperature on gas selectivity of CPM-200-In/Mg and CPM-200-In/Mg-X (-NH<sub>2</sub>, -OH, -N, -F).** We also investigated the effects of pressure and temperature on the gas selectivity ( $S_c$ ,  $S_{sc}$ ) of CPM-200-In/Mg and CPM-200-In/Mg-X (X = -NH<sub>2</sub>, -OH, -N, -F) in natural gas and post-combustion flue gas.

We explored the effects on  $S_s$  and  $S_{sc}$  of CPM-200-In/Mg and CPM-200-In/Mg-X, owing to the change of pressure. From Fig. S5 (ESI†), the maximum slope of increase of  $S_s$  and  $S_{sc}$  came from the increase in pressure ( $\leq 1$  bar) in the CPM-200-In/Mg -NH<sub>2</sub> (site 1 or site 2) mixture systems. For instance, when pressure was increased from 100 to 700 Torr at 298 K, the  $S_s$  of CPM-200-In/Mg-NH<sub>2</sub> (site 2) in natural gas mixture increased from 14 to 19, while the increases of the other frameworks were just less than 1.

We continued to explore the influence of temperature on the selectivity of CPM-200-In/Mg and CPM-200-In/Mg-X at 4 MPa and 1 bar, respectively, as plotted in Fig. 6 and Fig. S7 (ESI†). It is shown that the selectivity ( $S_s$ ,  $S_{sc}$ ) of the framework with functional groups would fall faster as the temperature increases in those mixture systems. Taking the natural gas mixture as an example, when the temperature increases from 273 K to 373 K at 4 MPa, the  $S_s$  of CPM-200-In/Mg-NH<sub>2</sub> (site 2) drops fastest from 30 to 10, while the decrease in the other frameworks is less than 3. Besides, the  $S_{sc}$  decrease is much larger than  $S_s$  of the framework when temperature increases. For instance, the  $S_{sc}$  of CPM-200-In/Mg-NH<sub>2</sub> (site 2) in the natural gas mixture system decreases from 53 to 8, while the decreases of  $S_s$  are just less than 20. That is to say, the effect brought on by temperature on the adsorption of CO<sub>2</sub> is much more obvious than that on H<sub>2</sub>S. We then found that the selectivity of the falling slope at high pressure area (4 MPa) is smaller than that at low pressure area (1 bar) as the temperature increases, as plotted in Fig. 6 and Fig. S7 (ESI†). For example, when temperature increased from 273 K to 373 K, the  $S_s$  of CPM-200-In/Mg-NH<sub>2</sub> (site 2) in the natural gas mixture decreased from 33 to 7 at 1 bar, while it decreased from 30 to 10 at 4 MPa. Thus, we can reduce the influence of temperature by raising the pressure.

## 4. Conclusions

In this work, the grand canonical Monte Carlo (GCMC) molecular simulation method and first-principle density functional theory (DFT) were employed to explore the adsorption performance of VOCs (HCHO, C<sub>2</sub>H<sub>4</sub>, CH<sub>4</sub>, C<sub>2</sub>H<sub>2</sub>, C<sub>3</sub>H<sub>8</sub>, C<sub>2</sub>H<sub>6</sub>, C<sub>2</sub>H<sub>3</sub>Cl, C<sub>2</sub>H<sub>2</sub>Cl<sub>2</sub>, CH<sub>2</sub>Cl<sub>2</sub> and CHCl<sub>3</sub>) and inorganic gases (HCN, SO<sub>2</sub>, NO, CO<sub>2</sub>, CO, H<sub>2</sub>S and NH<sub>3</sub>) in CPM-200-In/Mg. It was shown that CPM-200-In/Mg is more likely to adsorb the molecules with high polarizability (*i.e.* CO<sub>2</sub>, H<sub>2</sub>S, and SO<sub>2</sub>) at NTP and HCHO (VOC, 0.39 g g<sup>-1</sup>) as well as chlorine derivatives (C<sub>2</sub>H<sub>3</sub>Cl, C<sub>2</sub>H<sub>2</sub>Cl<sub>2</sub>, CH<sub>2</sub>Cl<sub>2</sub> and CHCl<sub>3</sub>).

The large adsorption capacities of the framework for HCN and HCHO could result from the strong interaction between adsorbates and metal centers, based on analyzing the radial distribution functions (RDF). The high adsorption capacities of C<sub>2</sub>H<sub>4</sub> and CH<sub>4</sub> of the framework for chlorine derivatives could be due to the existence of halogen bonding or strong electrostatic and VDW interactions, based on analyzing RDF and interaction energy.

By introducing functional groups ( $-\text{NH}_2$ ,  $-\text{OH}$ ,  $-\text{N}$ ,  $-\text{F}$ ) to CPM-200-In/Mg, we find that the introduction of basic groups ( $-\text{NH}_2$ ,  $-\text{OH}$  and  $-\text{N}$ ) can help to capture CO<sub>2</sub> and HCHO more effectively, while the  $-\text{F}$  polarity group is not helpful to the gas adsorption, but it is beneficial to CO<sub>2</sub> separation. It should be noted that the adsorption capacity of CPM-200-In/Mg-NH<sub>2</sub> (site 2) (245 cm<sup>3</sup> g<sup>-1</sup>) for CO<sub>2</sub> exceeded that of MOF-74-Mg (228 cm<sup>3</sup> g<sup>-1</sup>) at 273 K and 1 bar, and that for HCHO could reach 0.41 g g<sup>-1</sup>, which is almost twice that of 438-MOF. In addition, the introduction of the  $-\text{NH}_2$  basic group can greatly improve the decarburation and desulfurization abilities of CPM-200-In/Mg in H<sub>2</sub>S-CO<sub>2</sub>-CH<sub>4</sub> and SO<sub>2</sub>-CO<sub>2</sub>-N<sub>2</sub> ternary mixtures. For natural gas mixtures, the decarburation and desulfurization abilities of CPM-200-In/Mg-NH<sub>2</sub> (site 2) exceeded those of the MOF-74 series, while for post-combustion flue gas mixtures, the desulfurization ability of CPM-200-In/Mg-NH<sub>2</sub> (site 2) is still comparable to those of the MOF-74 series at 303 K and 4 MPa. Moreover, the selectivity ( $S_s$  and  $S_{sc}$ ) of CPM-200-In/Mg-NH<sub>2</sub> in those two ternary mixtures quickly decrease with increasing temperature and we can reduce the influence of the temperature by raising the pressure.

In conclusion, compared to the traditional MOFs, the main group heterometallic metal-organic frameworks can be an excellent material for the capture or separation of harmful gases. We hope the present work may serve as a theoretical supplement for experimental research, as well as guidance for the future developments of materials in gas adsorption, desulfurization and decarburation.

## Conflicts of interest

There are no conflicts to declare.

## Acknowledgements

The work was supported by the National Natural Science Foundation of China (No. 21373112, No. 21673079, No. U1301245 and No. 21263012), the Guangdong Natural Science Foundation (No. 2014A030313259 and No. 2016A030313518) and the Guangdong Science and Technology Planning Project (No. 2015A020216002 and No. 2014A020216045). In addition, we owe gratitude to Miss Min-min Ma for help with polishing the English.

## References

- P. Cosoli, M. Ferrone, S. Pricl and M. Fermeglia, Hydrogen sulfide removal from biogas by zeolite adsorption: part I. GCMC molecular simulations, *Chem. Eng. J.*, 2008, **145**, 86–92.
- D. Fairen-Jimenez, Y. J. Colón and O. K. Farha, *et al.*, Understanding excess uptake maxima for hydrogen adsorption isotherms in frameworks with rht topology, *Chem. Commun.*, 2012, **48**, 10496–10498.
- Y. S. Bae and R. Q. Snurr, Development and evaluation of porous materials for carbon dioxide separation and capture, *Angew. Chem., Int. Ed.*, 2011, **50**, 11586–11596.
- U. Mueller, M. Schubert and F. Teich, *et al.*, Metal-organic frameworks-prospective industrial applications, *J. Mater. Chem.*, 2006, **16**, 626–636.
- T. R. C. Van Assche and J. F. M. Denayer, Fabrication and separation performance evaluation of a metal-organic framework based microseparator device, *Chem. Eng. Sci.*, 2013, **95**, 65–72.
- N. Planas, A. L. Dzubak, R. Poloni, L.-C. Lin, A. McManus, T. M. McDonald, J. B. Neaton, J. R. Long, B. Smit and L. Gagliardi, The mechanism of carbon dioxide adsorption in an alkylamine-functionalized metal-organic framework, *J. Am. Chem. Soc.*, 2013, **135**, 7402–7405.
- S. N. Nobar and S. Farooq, Experimental and modeling study of adsorption and diffusion of gases in Cu-BTC, *Chem. Eng. Sci.*, 2012, **84**, 801–813.
- J. B. DeCoste and G. W. Peterson, Metal-organic frameworks for air purification of toxic chemicals, *Chem. Rev.*, 2014, **114**, 5695–5727.
- P. Kumar, K.-H. Kim and E. E. Kwon, *et al.*, Metal-organic frameworks for the control and management of air quality: advances and future direction, *J. Mater. Chem. A*, 2016, **4**, 345–361.
- D. Britt, D. Tranchemontagne and O. M. Yaghi, Metal-organic frameworks with high capacity and selectivity for harmful gases, *Proc. Natl. Acad. Sci. U. S. A.*, 2008, **105**, 11623–11627.
- E. Barea, C. Montoro and J. A. R. Navarro, Toxic gas removal-metal-organic frameworks for the capture and degradation of toxic gases and vapours, *Chem. Soc. Rev.*, 2014, **43**, 5419–5430.
- P. Silva, S. M. F. Vilela and J. P. C. Tomé, *et al.*, Multi-functional metal-organic frameworks: from academia to industrial applications, *Chem. Soc. Rev.*, 2015, **44**, 6774–6803.
- Q.-G. Zhai, X. Bu and C. Mao, *et al.*, Systematic and dramatic tuning on gas sorption performance in heterometallic metal-organic frameworks, *J. Am. Chem. Soc.*, 2016, **138**, 2524–2527.
- Q. Yang, A. D. Wiersum and P. L. Llewellyn, *et al.*, Functionalizing porous zirconium terephthalate UiO-66 (Zr) for natural gas upgrading: a computational exploration, *Chem. Commun.*, 2011, **47**, 9603–9605.
- C. G. Piscopo, F. Trapani and A. Polyzoidis, *et al.*, Positive effect of the fluorine moiety on the oxygen storage capacity of UiO-66 metal-organic frameworks, *New J. Chem.*, 2016, **40**, 8220–8224.
- Z. Qiao, N. Wang and J. Jiang, *et al.*, Design of amine-functionalized metal-organic frameworks for CO<sub>2</sub> separation: the more amine, the better?, *Chem. Commun.*, 2016, **52**, 974–977.

- 17 B. Delley, An all-electron numerical method for solving the local density functional for polyatomic molecules, *J. Chem. Phys.*, 1990, **92**, 508–517.
- 18 B. Delley, From molecules to solids with the DMol<sup>3</sup> approach, *J. Chem. Phys.*, 2000, **113**, 7756–7764.
- 19 S. L. Mayo, B. D. Olafson and W. A. Goddard, DREIDING: a generic force field for molecular simulations, *J. Phys. Chem.*, 1990, **94**, 8897–8909.
- 20 A. K. Rappé, C. J. Casewit and K. S. Colwell, *et al.*, UFF, a full periodic table force field for molecular mechanics and molecular dynamics simulations, *J. Am. Chem. Soc.*, 1992, **114**, 10024–10035.
- 21 Q. Yang, S. Vaesen and F. Ragon, *et al.*, A water stable metal–organic framework with optimal features for CO<sub>2</sub> capture, *Angew. Chem., Int. Ed.*, 2013, **52**, 10316–10320.
- 22 M. G. Martin and J. I. Siepmann, Transferable potentials for phase equilibria. 1. United-atom description of *n*-alkanes, *J. Phys. Chem. B*, 1998, **102**, 2569–2577.
- 23 M. J. Frisch, G. W. Trucks, H. B. Schlegel, G. E. Scuseria, M. A. Robb, J. R. Cheeseman, G. Scalmani, V. Barone, B. Mennucci and G. A. Petersson, *et al.*, Gaussian 09, revision A.01, Gaussian, Inc., Wallingford, CT, 2009, vol. 200.
- 24 H. Heinz and U. W. Suter, Atomic charges for classical simulations of polar systems, *J. Phys. Chem. B*, 2004, **108**, 18341–18352.
- 25 S. Alvarez, cartography of the van der Waals territories, *Dalton Trans.*, 2013, **42**, 8617–8636.
- 26 D. Dubbeldam, S. Calero, D. E. Ellis and R. Q. Snurr, Raspa: Molecular Simulation Software for Adsorption and Diffusion in Flexible Nanoporous Materials, *Mol. Simul.*, 2016, **42**, 81–101.
- 27 M. Du, M. Chen and X. Wang, *et al.*, Versatile mesoporous DyIII coordination framework for highly efficient trapping of diverse pollutants, *Inorg. Chem.*, 2014, **53**, 7074–7076.
- 28 Z. Li, F. Liao and F. Jiang, *et al.*, Capture of H<sub>2</sub>S and SO<sub>2</sub> from trace sulfur containing gas mixture by functionalized UiO-66 (Zr) materials: A molecular simulation study, *Fluid Phase Equilib.*, 2016, **427**, 259–267.
- 29 X. Peng and D. Cao, Computational screening of porous carbons, zeolites, and metal organic frameworks for desulfurization and decarburization of biogas, natural gas, and flue gas, *AICHE J.*, 2013, **59**, 2928–2942.
- 30 R. Luebke, J. F. Eubank and A. J. Cairns, *et al.*, The unique rht-MOF platform, ideal for pinpointing the functionalization and CO<sub>2</sub> adsorption relationship, *Chem. Commun.*, 2012, **48**, 1455–1457.
- 31 B. Zheng, J. Bai and J. Duan, *et al.*, Enhanced CO<sub>2</sub> binding affinity of a high-uptake rht-type metal–organic framework decorated with acylamide groups, *J. Am. Chem. Soc.*, 2011, **133**, 748–751.
- 32 Z. Lu, J. Bai and C. Hang, *et al.*, The Utilization of Amide Groups To Expand and Functionalize Metal–Organic Frameworks Simultaneously, *Chem. – Eur. J.*, 2016, **22**, 6277–6285.
- 33 I. Spanopoulos, I. Bratsos and C. Tampakis, *et al.*, Exceptional gravimetric and volumetric CO<sub>2</sub> uptake in a palladated NbO<sub>4</sub>-type MOF utilizing cooperative acidic and basic, metal–CO<sub>2</sub> interactions, *Chem. Commun.*, 2016, **52**, 10559–10562.
- 34 L. Hamon, H. Leclerc and A. Ghoufi, *et al.*, Molecular insight into the adsorption of H<sub>2</sub>S in the flexible MIL-53 (Cr) and rigid MIL-47 (V) MOFs: infrared spectroscopy combined to molecular simulations, *J. Phys. Chem. C*, 2011, **115**, 2047–2056.
- 35 D. Kim, T. B. Lee and S. B. Choi, *et al.*, A density functional theory study of a series of functionalized metal–organic frameworks, *Chem. Phys. Lett.*, 2006, **420**, 256–260.
- 36 Z. P. Chen, L. X. Ling, B. J. Wang and H. L. Fan, *et al.*, Adsorptive desulfurization with metal–organic frameworks: a density functional theory investigation, *Appl. Surf. Sci.*, 2016, **387**, 483–490.
- 37 Z. Tian, S. Dai and D.-E. Jiang, Site partition: turning one site into two for adsorbing CO<sub>2</sub>, *J. Phys. Chem. Lett.*, 2016, **7**, 2568–2572.
- 38 J. Zhang, X. Zheng and C. Liu, *et al.*, Probing the chemical bonding and electron structure of the benzoate model for Fe-MoF-5, in: MRS Proceedings, Cambridge University Press, 2013, p. mrss13-1548.
- 39 H. M. Wen, H. Wang and B. Li, *et al.*, A Microporous Metal–Organic Framework with Lewis Basic Nitrogen Sites for High C<sub>2</sub>H<sub>2</sub> Storage and Significantly Enhanced C<sub>2</sub>H<sub>2</sub>/CO<sub>2</sub> Separation at Ambient Conditions, *Inorg. Chem.*, 2016, **55**(15), 7214.